

Direct measurement of the adiabatic temperature change and study of the reversibility in the magnetocaloric effect of $Fe_{0.49}Rh_{0.51}$

Author: Adrià Gràcia Condal

Facultat de Física, Universitat de Barcelona, Diagonal 645, 08028 Barcelona, Spain.

(Dated: June 13, 2014)

Abstract: The adiabatic temperature change (ΔT_{ad}) around a magnetic field-induced first order phase transition can vary significantly when the field is applied for the first time or under further applications. With the purpose to measure directly ΔT_{ad} , I designed a suitable experimental setup and used it to analyze the magnetocaloric effect of a sample of $Fe_{0.49}Rh_{0.51}$ under a field-cycling between 0 and 2 Tesla.

I. INTRODUCTION

The magnetocaloric effect (MCE) describes the adiabatic temperature change of a material when subjected to a sudden variation of an external magnetic field and, from another point of view, it is related to the entropy variation when the magnetic field is changed isothermally. The MCE was first discovered in 1881 by E. Warburg, but a major advance occurred at the late 1920s, when Debye and Giauque independently suggested that the MCE could be used to reach extremely low temperatures via adiabatic demagnetization [1]. However, this effect was only known to be significant at very low temperatures. A second major advance took place in 1997 with the discovery by Pecharsky and Gschneidner of an intermetallic Gd-Si-Ge material that exhibits a large adiabatic temperature change around room temperature. This compound was denoted to display a giant magnetocaloric effect (GMCE) [2].

The presence of GMCE is usually related to a first order phase transition of the material. Under the application of an external magnetic field, the material experiences a phase transition which involves a large entropy change. In most cases, isothermal application of a magnetic field reduces the material's entropy, and the adiabatic application of a magnetic field increases its temperature. This is known as the 'conventional' MCE. However, the reverse situation is also possible. There are some materials in which isothermal application of a magnetic field increases the material's entropy, and the adiabatic application of a magnetic field reduces its temperature. This effect is referred as 'inverse' MCE [3].

To study the MCE, I performed direct measurements of the adiabatic temperature change (ΔT_{ad}) of a sample of $Fe_{0.49}Rh_{0.51}$ under an external magnetic field between 0 and 2 Tesla. This material presents a field-induced first order magnetic phase transition, with an entropy change (ΔS), between a low temperature antiferromagnetic state (AFM) and a high temperature ferromagnetic one (FM) [4]. Moreover, due to the strong coupling between magnetic and structural properties, the field-induced phase transition involves a structural change of the sample [5], resulting in a thermal hysteresis. Therefore, the measured magnitude ΔT_{ad} is strongly dependent upon a cycling variation of the magnetic field.

II. EXPERIMENTAL

A. Experimental setup

The experimental setup is schematically represented in figure 1.

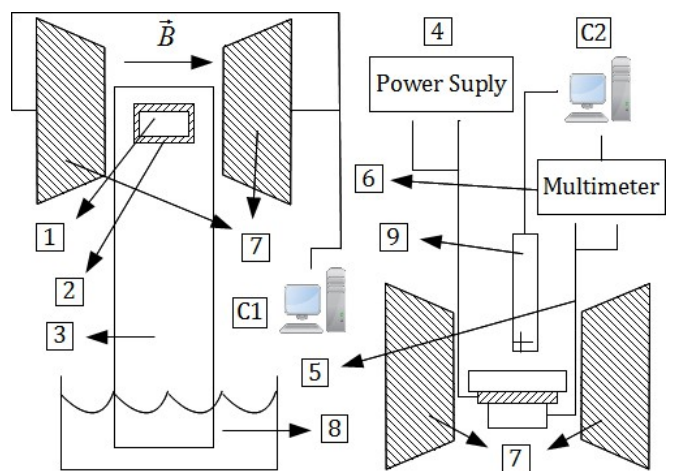


FIG. 1: Front view (left) and top view (right) of the experimental setup. 1: $Fe_{0.49}Rh_{0.51}$ sample, 2: Thermobattery, 3: Copper bar, 4: Power supply, 5: Thermocouple, 6: Multimeter, 7: Electromagnet, 8: Heat sink of H_2O , 9: Hall probe, C1: Computer, C2: Thermocouple and Hall probe recording computer

The sample ($3,1 \times 3,3 \times 6,6 \text{ mm}^3$, 468,715 mg) (1) is attached onto one side of the thermobattery (2), and a copper bar (3) onto the other side. The thermobattery (MELCOR: *OptoTEC*TM series), consisting of 24 Bi_2Te_3 thermocouples on a surface of $0,5 \times 0,5 \text{ cm}^2$, is used to heat or cool down the sample depending on the applied voltage with the power supply (4) ($-0,2 \text{ V} < V_{therbat} < 1 \text{ V}$). The sample temperature is directly measured with a copper-constantan T type thermocouple (5), which was embedded inside a hole centered in the sample. The output of the thermocouple was continuously monitored by a multimeter (6) that electronically compensates for the reference junction. The temperature of the reference junction was selected as the best to reproduce the temperature of water and ice mixture. A silicone heat-conducting paste (HTS) was used to assure a good ther-

mal contact between the thermocouple and the sample. The sample, the thermobattery and the top of the copper bar where wrapped together with Teflon tape, in order to minimize the heat exchange between the sample and the environment. The whole system is subjected using the two poles of the computer-controlled electromagnet (7). The thermal bath (8), which is in contact with the bottom of the copper bar (3) acts as a heat sink. The magnetic field was controlled by the electromagnet computer (C1), and was measured by a Hall probe (9) next to the sample. Both, the thermocouple and the Hall probe data, were recorded by a second computer (C2).

B. Calorimetric measurements

The isothermal entropy change at the phase transition was determined by isofield DSC measurements made on the same sample of $Fe_{0.49}Rh_{0.51}$ I used to measure ΔT_{ad} . DSCs are suitable to study materials that undergo a first order phase transition as they enable us to determine the latent heat of the transition [6]. These measurements were performed for the temperature range $T \approx 275 - 340$ K, where the sample undergoes the phase transition (inset of figure 2), with a transition entropy change of $10,5$ J/Kkg. To complete these calorimetric measurements I used the specific heat data obtained from [7], which covers a temperature range $T \approx 2 - 380$ K. Using the equation:

$$S(T_{fin}, H) - S(T_{ref}, H) = \int_{T_{ref}}^{T_{fin}} \frac{C_p(T)}{T} dT, \quad (1)$$

where $C_p(T)$ is the specific heat, I calculated the isofield entropy for the sample covering the temperature range $T \approx 2 - 275$ K. As both measurements give information of different temperature ranges, in figure 2 I plotted the entropy curves obtained by combining both calorimetric measurements. It is important to notice that above or below the phase transition temperature range, the specific heat is independent of the magnetic field. Therefore, in figure 2 the entropy curves coincide outside of this region. Furthermore, the application of the magnetic field shifts the phase transition to lower temperatures at a rate of $\sim 8,5$ K/T, but does not significantly affect the width of the thermal hysteresis.

C. Experimental measurement protocols

To measure properly ΔT_{ad} it is of major importance to achieve as good as possible adiabatic conditions during the measurement time and, secondly, to control the state (AFM or FM) of the sample at the beginning of each measurement. For the first goal, if we take into account the exponential Newton-law for thermal equilibrium [8]:

$$T^{sample} = T_{room-temp} + (T_0^{sample} - T_{room-temp})e^{-\frac{t}{\tau}} \quad (2)$$

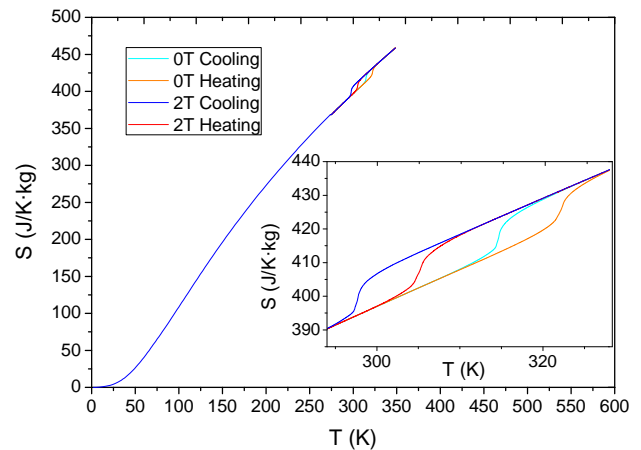


FIG. 2: Isofield heating and cooling entropy curves for 0 Tesla (orange and cyan, respectively) and 2 Tesla (red and blue) between 2 and 340 Kelvin for the sample of $Fe_{0.49}Rh_{0.51}$. Inset of the phase transition area for all entropy curves.

where τ is the characteristic time of relaxation of the sample and t is the time needed to apply the magnetic field, it is possible to determine how accurate are the adiabatic conditions. For the experimental setup I used, $t \approx 10^{-2}\tau$. Therefore, it is reasonable to assume adiabatic conditions during the first cycles of the magnetic field during the measurement time. The second goal can be easily solved by heating or cooling down the sample far over the transition region, as schematized in figure 3.

In both protocols, the computer records the value from the Hall probe and from the thermocouple every 0,4 seconds, and each field cycle took 8 seconds.

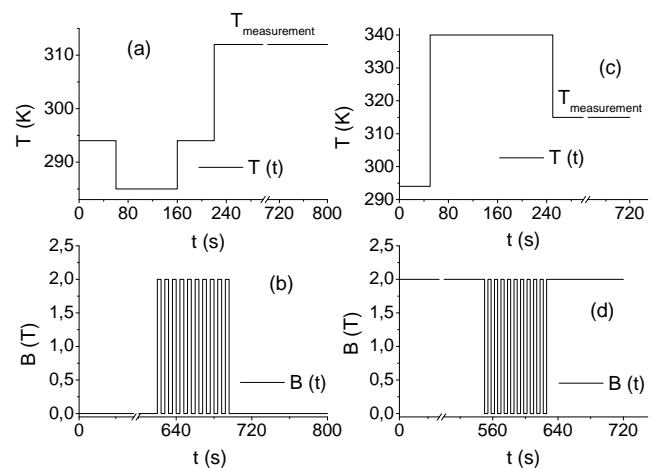


FIG. 3: Schematic representation of the heating (left side) and cooling (right side) protocols. For each one, I represented the sample temperature and the electromagnet magnetic field, both as a function of time.

The heating protocol is schematically represented in figure 3, (a) and (b). Without magnetic field, the sample is completely transformed to the AFM phase by cooling it down. When the temperature stabilizes around 285 K,

the power supply is disconnected and the sample returns to room temperature. Then, the sample is heated up until the desired measurement temperature and, when the temperature stabilizes, 10 periods of field-cycling between 0 and 2 Tesla are performed. Finally, at the end of the cycling, the field is removed and the sample returns to the measurement temperature.

The cooling protocol is schematically represented in figure 3, (c) and (d). Applying a field of 2 Tesla, the sample is completely transformed to the FM phase by heating it up. When the temperature stabilizes around 340 K, the sample is cooled down until the desired measurement temperature. Then, 10 periods of field-cycling between 2 and 0 Tesla are performed. Finally, at the end of the cycling, the field is maintained at 2 Tesla and the sample returns to the measurement temperature.

III. RESULTS AND DISCUSSION

In order to assure proper adiabatic conditions during the measurement time, I used the data obtained for the first four field-cycles of each measurement. From here on, I will refer to a field ramp as a variation of the field, whether it is from 0 to 2 Tesla or vice versa. Therefore, a field-cycle consists of two opposite field ramps (see figure 3, (b) and (d)).

Figure 4 shows an example of the data recorded by the computer.

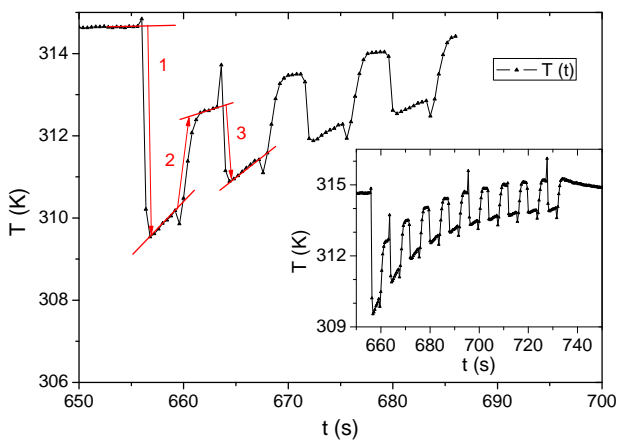


FIG. 4: First four cycles of a measurement obtained for the heating protocol. Inset: Total measure obtained.

The arrows represent each ramp measured, and their reference temperature is determined by the start-point of each one. Both arrows 1 and 3 show a cooling of the system, while arrow 2 represents a heating.

The first ramp ΔT_{ad} values with their error bars, compared with the indirect data obtained from the entropy curves, are plotted at the top of figure 5. For the calorimetric measurements, I have considered an error of 5% for the specific heat of the sample, which taking into

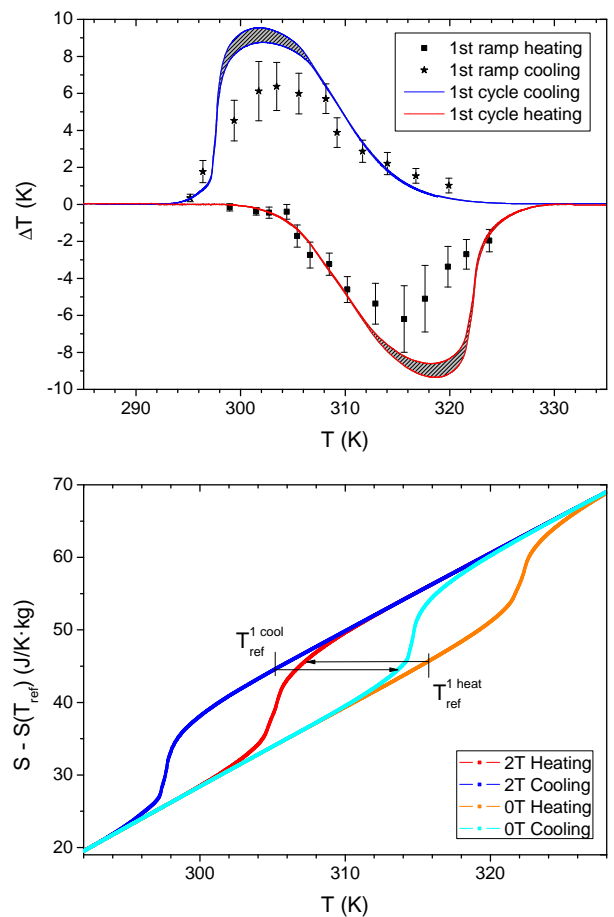


FIG. 5: Top: First ramp experimental values of ΔT_{ad} for both protocols compared with the indirect data from the entropy curves. Bottom: Isofield entropy curves around the phase transition.

account equation (1) implies an error for the entropy and the expected ΔT_{ad} . This error is represented in the graphic as the shaded area between the curves for both heating and cooling protocols (red and blue lines in figure 5, respectively). For the experimental measurements, error bars are computed from the reproducibility of the values under three independent measurements. Lower panel in figure 5 shows an entropic scheme around the field-induced phase transition, in order to visualize the origin of ΔT_{ad} for the first field ramp. The arrows represent the first ramp predicted values of ΔT_{ad} for both protocols. For the cooling protocol, all measurements start at the 2 Tesla cooling curve, which represents the transition from the FM to the AFM state under a 2 Tesla field. The measurement temperature is where the start-point of the arrow is located (see figure 5). Following the cooling protocol (figure 3), when the field is removed the system will experience a phase transition. In this case, the end-point of the arrow is located on the 0 Tesla cooling curve, as both correspond to the same transition direction (from FM to AFM), and the temperature of the system will increase. On the other hand, for the heating

protocol the measurement starts at the 0 Tesla heating curve, which corresponds to the transition from AFM to FM state without field. As indicates this protocol (figure 3), when the field is applied the system will experience the reverse phase transition. Then, the end-point of the arrow is located on the 2 Tesla heating curve, as both correspond to the transition direction from AFM to FM state, implying a decrease of its temperature. Notice that the MCE in $Fe_{0.49}Rh_{0.51}$ is inverse, hence adiabatic application of the field cools the sample while removal of the field results in an increase of temperature.

Although there is a good agreement between ΔT_{ad} obtained from indirect measurements and that directly measured, the experimental data are systematically lower, specially around the maximum and the minimum. The experimental results obtained represent correctly the width of the expected transition range for both protocols and exhibit a similar maximum (and minimum) absolute value ($\sim 6,4$ K for cooling and $\sim 6,2$ K for heating), while the expected ones are between $8,8 - 9,6$ K for cooling and $8,6 - 9,4$ K for heating protocols.

The subsequent ramps ΔT_{ad} values with their error bars for heating (a) and cooling (b) protocols, compared with the indirect data obtained from the entropy curves, are plotted in figure 6. The same error for the specific heat measurements (5%) has been taken into account to calculate the indirect data for the subsequent ramps, leading to the shaded area in both graphics (a) and (b) of figure 6. Lower panel of the figure shows an entropic scheme around the phase transition, in order to visualize the origin of the reversible part of ΔT_{ad} for both measurement protocols. The arrows represent both the first ramp ΔT_{ad} predicted values and the subsequent ones. For the cooling protocol, after the first field ramp the system is on the 0 Tesla cooling curve. When the field is applied again, the sample will experience a new phase transition to the FM state and, therefore, the end-point of the arrow will be located on the 2 Tesla heating curve, as it corresponds to the transition direction from the AFM to the FM state. If the field is removed a second time, the system will return to the 0 Tesla cooling curve, and if it is applied again, it will evolve to the 2 Tesla heating curve. Consequently, for all subsequent ramps, the system will repeat the 1-arrow. On the other hand, for the heating protocol the system is on the 2 Tesla heating curve after the first field ramp. When the field is removed again, the sample will experience the reverse phase transition. Therefore, it will transform to the AFM state, and the end-point of the arrow will be located on the 0 Tesla cooling curve, as it corresponds to the transition direction from the FM to the AFM state. If the field is applied a second time, the system will return to the 2 Tesla heating curve, and if it is removed again, it will evolve to the 0 Tesla cooling curve. Consequently, for all subsequent ramps, the system will repeat the 1'-arrow. It is important to notice that, for the same field ramp of both protocols (for example, the second ramp), the directions of the transitions are the opposite of one another. In this

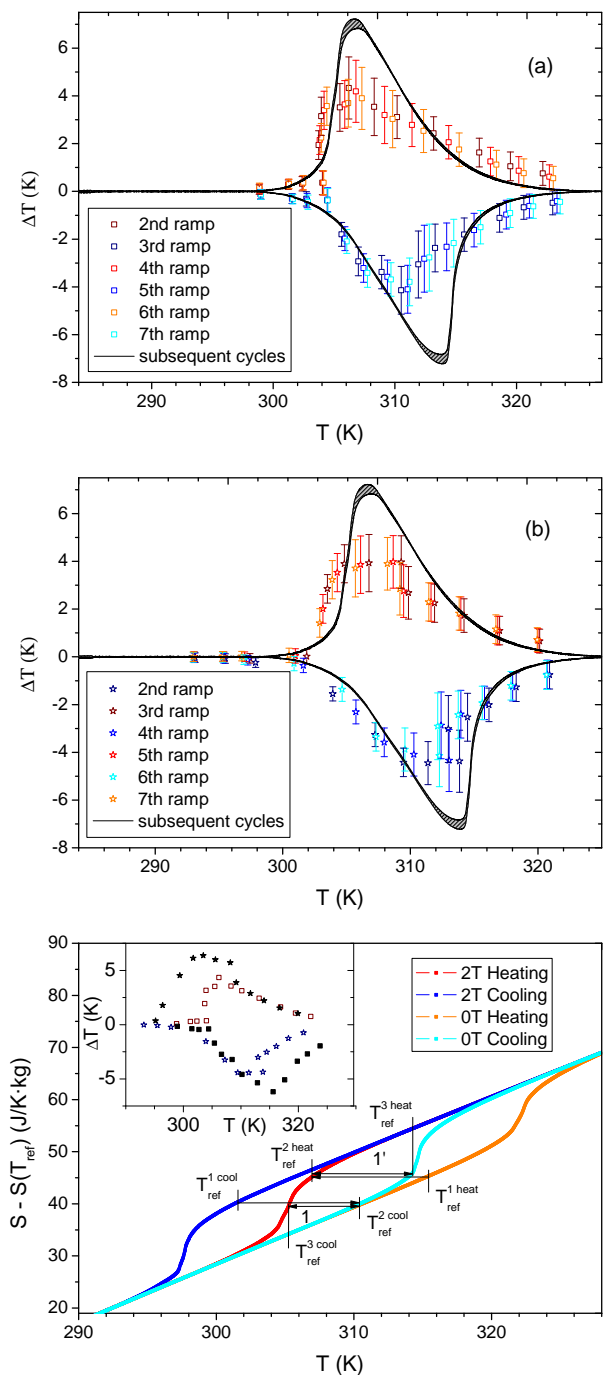


FIG. 6: Subsequent ramp experimental values of ΔT_{ad} for heating (a) and cooling (b) protocols, compared with the indirect data from the entropy curves. Bottom: Isofield entropy curves around the phase transition. Inset: First and second ramp experimental values for both protocols.

particular case, the second ramp implies a temperature decrease for the cooling protocol, while it implies an increase for the heating protocol (figure 6).

Although there is a good agreement between ΔT_{ad} obtained from indirect measurements and those directly measured, the experimental data are systemati-

cally lower, specially around the maximum and the minimum. For both graphics (a) and (b), the width of the experimental measures is in good agreement with the expected values. For the heating protocol, the maximum and minimum values are $\sim 4,3 K$ and $\sim -4,1 K$ respectively, while the expected ones are between $6,8 - 7,2 K$ for both (in module). Furthermore, for the cooling protocol, the maximum and minimum values are $\sim 4 K$ and $\sim -4,5 K$ respectively, while the expected ones are the same as for the heating protocol. A smaller deviation is observed at high temperatures for both graphs (a) and (b), where the measured ΔT_{ad} approaches to zero more gradually than expected, but the error bars of both cover the expected values. Moreover, for both protocols a better agreement with the indirect values for the second field ramp measurements is observed, compared with the other ramps. Finally, it is of special significance to compare the dispersion of the ramps which exhibit the same sign of ΔT_{ad} for both protocols separately. From both graphics (a) and (b), there is a major dispersion of the points around the maximum and the minimum than far away of them. As it can be deduced from the entropic curves of the figure, there should be no dispersion of this values if the measurements fulfilled adiabatic conditions.

Finally, it is interesting to analyze how reversible is the field-induced phase transition along the transition temperature range. As explained before, while analyzing the arrows of the entropy scheme of figure 6, all measurements following the cooling (heating) protocol start at the 2 Tesla cooling (0 Tesla heating) curve. For the cooling protocol, the start-point of the first field ramp arrow (T_{ref}^{1cool} , at the figure) is different of the start-point at 2 Tesla of 1-arrow (T_{ref}^{3cool}). The same observation is valid for the heating protocol, where the start-point of the first field ramp arrow is T_{ref}^{1heat} , and T_{ref}^{3heat} for the 1'-arrow. Therefore, as mentioned in [9], it is better to compare the first and the subsequent ramps that have the same 2 Tesla (for the cooling protocol) or 0 Tesla (for the heating protocol) reference temperature. At the inset of the entropy scheme of figure 6, experimental data for the first and second ramps for both protocols are plotted together, where error bars of the data have been removed in order to simplify the figure. It is important to point

out that for the maximum and the minimum values of the first field ramp, there is a small reversibility. While for the maximum and minimum values of the second ramp, there is a significant magnitude of the first field ramp. This observations are coherent with the entropy scheme, as it is easy to deduce that the first field ramp is always bigger or equal than the reversible part.

Notice that the first ramp cooling and the second ramp heating coincide for the approximate temperature range $T > 310 K$, while the first ramp heating and the second ramp cooling coincide for the range $T < 310 K$. Therefore, the optimal working temperature for solid-state refrigeration is around $T \approx 310 K$.

IV. CONCLUSIONS

A simple experimental setup able to measure the adiabatic temperature change for all the transition temperature range of $Fe_{0.49}Rh_{0.51}$ was designed and built. The setup has been used to measure ΔT_{ad} induced by a magnetic field over a broad temperature range (results shown in figure 5 for the first ramp, and figure 6 for the subsequent ones). While it was assumed for long time that the magnetocaloric effect in Fe-Rh was not reversible [2], present results demonstrate an excellent reproducibility. Therefore, with these measures it has been proved that $Fe_{0.49}Rh_{0.51}$ compound is of great interest for further investigation in solid-state refrigeration. On the other hand, to enhance the accuracy of the experimental measurements would be desirable an improvement of the experimental setup adiabatic conditions.

Acknowledgments

I would specially like to thank Lluís Mañosa and Enric Stern-Taulats for their constant help. Without their guidance and patience, I would have never finished this project. Last but not least, I want to use the last lines of this paper to express an immense gratitude to all my friends and family, as they always trusted in me unhesitatingly.

-
- [1] A.M. Tishin and Y.I. Spichkin "The Magnetocaloric Effect and its Applications" Institute of Physics, Bristol (2003).
 - [2] V.K. Pecharsky et al. Phys.Rev.Lett., **78**, 4494 (1997).
 - [3] Lluís Mañosa et al. J.Mater.Chem. A, **1**, 4925 (2013).
 - [4] M.P. Annaorazov et al. Cryogenics, **32** No. 10, p.867-872 (1992).
 - [5] S.O. Mariager et al. Phys.Rev.Lett., **108**, 087201 (2012).
 - [6] Jordi Marcos et al. Rev.Sci.Instrum., **74** No. 11, p.4768-4771 (2003).
 - [7] David W. Cooke et al. Phys.Rev.Lett., **109**, 255901 (2012).
 - [8] David G. Alonso "Magnetism and structure in functional alloys" PhD Thesis, University of Barcelona (2014).
 - [9] K.P. Skokov et al. J.Alloys Comp., **512**, p.310-317 (2013).